Bollettino di Geofisica Teorica ed Applicata Vol. 58, n. 3, pp. 205-216; September 2017
DOI 10.4430/bgta0196

Characterization of the Houze-Vali iron ore in the centre of Iran using magnetic gradient tensor data

N. Moghtaderi, B.H. Dehkordi and B. Oskooi

Geomagnetism Group, Institute of Geophysics, University of Tehran, Iran

(Received: July 4, 2016; accepted: June 12, 2017)

ABSTRACT This paper presents a case study on the use of Normalized Source Strength (NSS) to interpret magnetic gradient tensor data. This application was made to explore an iron ore deposit in the Houze-Vali area, located near Ardakan City in the centre of Iran. The source location was estimated by using Euler deconvolution of Total Magnetic Intensity and NSS data, after an upward continuation of 15 m. In general, the NSS is relatively insensitive to the magnetization direction, but it provides more reliable information in comparison with compared to the 3D analytic signal technique. According to the NSS results, the source can be approximated by an N60°W striking contact with its top at a depth of 102 m, which is consistent with the sampling results.

Key words: Normalized Source Strength (NSS), Euler deconvolution, 3D analytic signal, iron ore deposit, Houze-Vali, Iran.

1. Introduction

Magnetic surveys are very useful to detect magnetic anomalies related to ore deposits and mineralized environments and many methods have been developed to evaluate the source parameters. While Total Magnetic Intensity (TMI) is the most common data type acquired during magnetic surveys, vector components of the field and magnetic gradient tensor components can be derived from gridded TMI data, of sufficiently high quality and adequate sampling density, on a horizontal plane by using the Fast Fourier Transform (FFT) algorithm [Lourenço and Morrison (1973); see also chapter 12 of Blakely (1995) and Schmidt and Clark (1998) for details]. Clark (2012a) gives an algorithm for correcting measured TMI data to obtain a true potential field, which is important for the accurate calculation of vector and tensor components when large anomalies occur within the surveyed area. Except in special cases, e.g., large-scale regional anomalies (Pilkington and Beiki, 2013), the presence of significant remnant magnetization can lead to erroneous interpretations of magnetic data. Pilkington and Beiki (2013) proposed two approaches to deal with this issue without having measurements of the rock properties.

In the first approach, the total magnetization vector direction is estimated based on the magnetic data. There are several methods to carry out this estimation (e.g., Helbig, 1963; Roest and Pilkington, 1993; Schmidt and Clark, 1998; Phillips, 2005; Dannemiller and Li, 2006; Gerovska *et al.,* 2009; Pilkington and Beiki, 2013). Clark (2014) published a comprehensive review of methods to estimate total and remnant magnetizations of geological sources.

The second approach is based on the derivation of quantities that are insensitive to the direction of the magnetization (Roest *et al.,* 1992; Thurston and Smith, 1997; Stavrev and Gerovska, 2000; Sertcelik and Kafadar, 2012). The NSS (Beiki *et al.*, 2012; Clark, 2012a) falls into this category.

In this paper, we have applied the Normalized Source Strength (NSS) and the Analytic Signal Amplitude (ASA), calculated from a TMI survey made on the Houze-Vali iron ore deposit to interpret some main features of that area. Section 2, briefly describes the geology of this area. Section 3 describes the survey specifications and the mathematical methods used to analyze the data, including a brief discussion of the ASA and NSS, followed by a discussion of the results in Section 4 and conclusions in Section 5.

2. Geological setting

The Houze-Vali study area, located close to Toot Village about 50 km NE of Ardakan City in Yazd Province, Iran, has an area of about 40 km^2. The study area is almost completely flat and has a consistent dip to the N-NW. The major geomorphologies on the map are low hills, inselbergs, sand dunes, transverse barchans, piedmont plain, alluvial fans, and playa lakes.

According to the 1:100,000 geological map, as shown in Fig. 1, the most important lithological units, arranged in order of increasing age, are as follows:

A - the Rizo formation (PC_r), comprising sequences of sedimentary and igneous rocks, such as rhyolite, tuff, silt, sandstone, limestone-dolomite, shale and pyroclastic rocks;

B - Precambrian granite (Gr), which intruded the Rizo Formation and created the iron ore deposit through metasomatic processes within the contact aureole;

C - Quaternary alluvium (Q), comprising a complex assemblage of alluvial fan, terraces, silt-clay and clay-silt deposits.

There are two major azimuths, NW-SE and the NE-SW, for the faults of the area.

3. Data and method

3.1. Magnetic data

Ground magnetic data were acquired over an area of 1.8 km^2 along 14 N-S oriented lines, with a line spacing of 20 m and an along-line sampling interval of 5 m. The data were interpolated onto a regular 5×5 m^2 grid using the Geosoft minimum curvature gridding algorithm and the gradient tensor elements were calculated from the gridded TMI values by Fourier filtering [see Chapter 12 of Blakely (1995) for the relevant theory].

3.2. Analytic Signal Amplitude (ASA)

The analytic signal, introduced by Nabighian (1972, 1974) and broadened by Nabighian (1984) and Roest *et al.* (1992), is derived from a combination of the horizontal and vertical gradients of a magnetic anomaly. While the 2D analytic signal amplitude is independent of the magnetization direction, in general, the 3D case varies with the direction of the magnetization vector, as shown by Salem *et al.* (2002). The 3D analytic signal of a potential field Φ and its ASA, also commonly called the total gradient amplitude (for a complete explanation of the symbols see the Appendix),

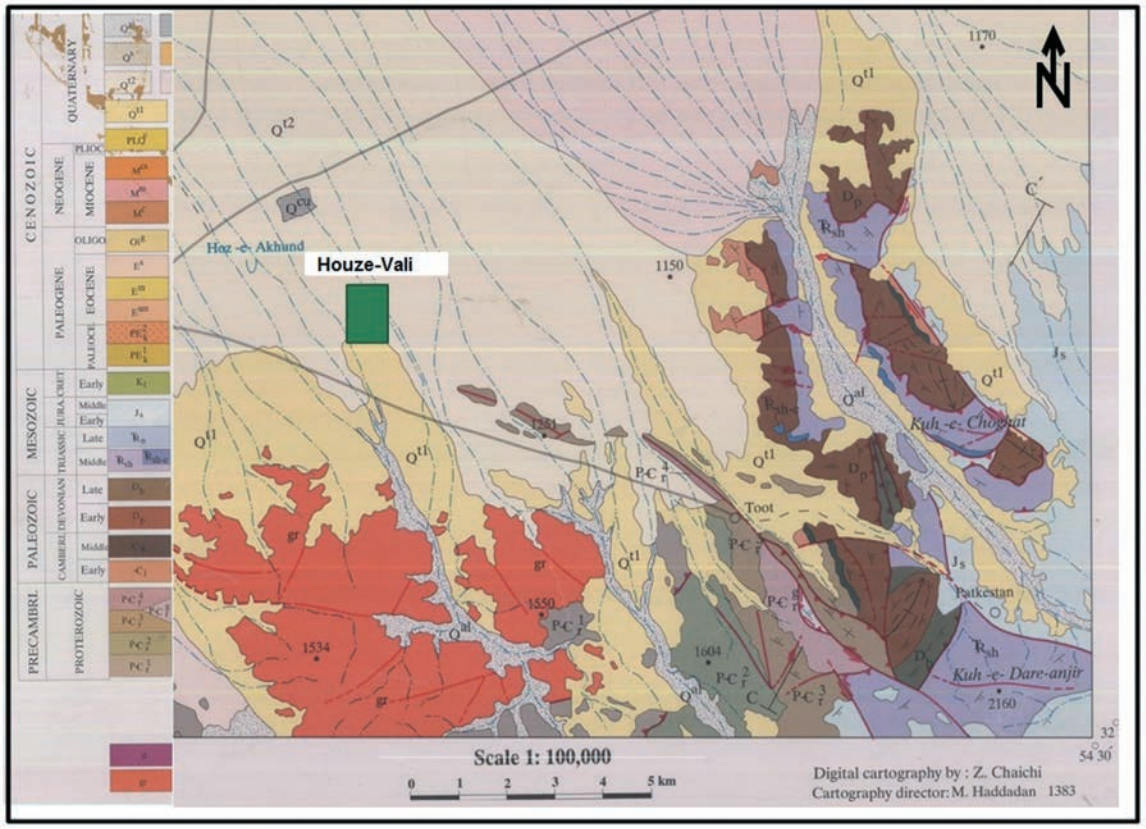

Fig. 1 - The 1:100,000 geological map of Houze-Vali region.

are given by, respectively (Bastani and Pedersen, 2001):

$$A(x,y) = \frac{\partial \Phi(x,y)}{\partial x} + \frac{\partial \Phi(x,y)}{\partial y} + i\frac{\partial \Phi(x,y)}{\partial z}, \quad (1)$$

$$|A(x,y)| = \sqrt{\left[\frac{\partial \Phi(x,y)}{\partial x}\right]^2 + \left[\frac{\partial \Phi(x,y)}{\partial y}\right]^2 + \left[\frac{\partial \Phi(x,y)}{\partial z}\right]^2}. \quad (2)$$

3.3. Normalized source strength (NSS)

Analysis of the magnetic gradient tensor refers to Wilson (1985). Beiki *et al*. (2012) and Clark (2012a), introduced the NSS parameter, which is independent of magnetization direction for 2D and for simple 3D sources (such as spheres, compact sources that can be adequately represented by a point dipole and axially-magnetized thin pipes) and only weakly dependent on magnetization direction otherwise. The NSS is calculated from the eigenvalues of the magnetic or gravity gradient tensor:

$$\mu = \sqrt{-\lambda_2^2 - \lambda_1\lambda_3}, \quad (3)$$

where $\lambda_1 \geq \lambda_2 \geq \lambda_3$ are the eigenvalues of the gradient tensor in non-increasing order.

For elementary sources, the generalized form of the NSS can be expressed as:

$$\mu = \frac{qC_m}{|\boldsymbol{r} - \boldsymbol{r_0}|^{|n|}}\ , \tag{4}$$

where μ is measured in nT/m, Cm = 100 nTm/A and $\boldsymbol{r}$ and $\boldsymbol{r_0}$ are the locations of the observation and source point, in units of metres. The parameters n and q are the structural index and the geometry factor of simple magnetic sources, respectively [for more details: Table 1 in Beiki *et al*. (2012)]. Regarding Eq. 4, Beiki *et al*. (2012) estimated source parameters according to the Euler deconvolution of the NSS as a non-harmonic homogeneous function. Derivatives of the eigenvalues can be used to calculate the NSS derivatives as:

$$\frac{\partial \mu}{\partial \alpha} = -\frac{\frac{\partial \lambda_3}{\partial \alpha}\lambda_3 + 2\frac{\partial \lambda_2}{\partial \alpha}\lambda_2 + \frac{\partial \lambda_3}{\partial \alpha}\lambda_1}{2\mu}\ , \qquad \alpha = x, y, and\ z \tag{5}$$

They can also be successfully used to calculate the NSS derivatives, which are needed to accomplish the Euler deconvolution. Derivatives of the eigenvalues that occur in Eq. 5 can be calculated from the gradient tensor elements, using algorithms provided by Beiki *et al*. (2012) and Clark (2012a). A square window, centred at the location of the maximum of the NSS, is then chosen and increased in size to reach a predefined limit. The best solution is thus chosen based on minimum values of the uncertainties of the estimated parameters (Beiki, 2010; Beiki *et al*., 2012).

4. Discussion

The residual TMI map (Fig. 2a) shows four anomalies, labelled A, B, C and D, where anomaly A is broader and smoother than the other anomalies, suggesting a deeper source. Upward continuation of the TMI grid by 15 m (Fig. 2b), 100 m (Fig. 2c) and 700 m (Fig. 2d) confirms that the source of anomaly A is a deep body, which is interpreted to represent the metasomatized aureole of the granite. After upward continuation by 100 m, A remains as a major anomaly, while B, C and D have disappeared (see Fig. 2c). This suggests that anomalies B, C and D arise from shallow sources. After upward continuation by 700 m, anomaly A becomes broader and more diffuse, its amplitude is greatly reduced and its centre shifts southwards, suggesting that the magnetic body plunges to the south. Upward continuation by more than 700 m suppresses anomaly A almost entirely, indicating that the magnetic source has a limited depth.

Fig. 3a shows the calculated second vertical derivative of the measured TMI. In this map, anomalies B, C and D are relatively more prominent than anomaly A, and they appear to be resolved into complex patterns, suggesting multiple shallow sources that possibly represent blocks of magnetite ore dispersed within the overburden. It is worth noting that they are shallower anomalies than A. Because the derivatives of the field are relatively noisy, the grid was upward continued by 15 m before calculating the 3D analytic signal amplitude (total gradient). Based on the ASA map, the estimated horizontal dimensions of the source of anomaly A are 380 by 600 m. The strong magnetic contrast between the country rock and the source of anomaly A suggests a high magnetite content of its source.

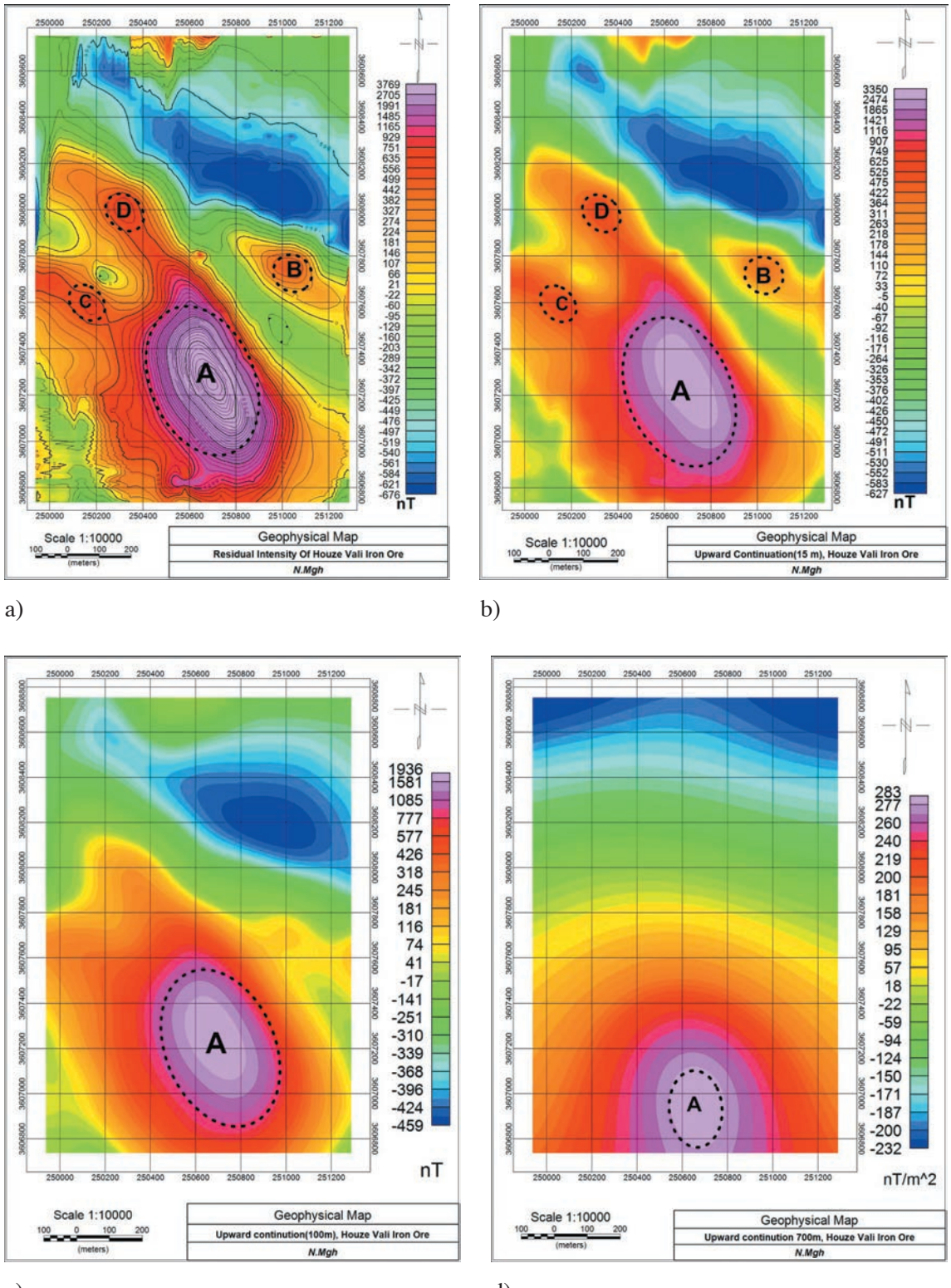

Fig. 2 - a) Residual magnetic intensity of Houze-Vali iron ore; b) upward continuation 15 m; c) upward continuation 100 m; d) upward continuation 700 m.

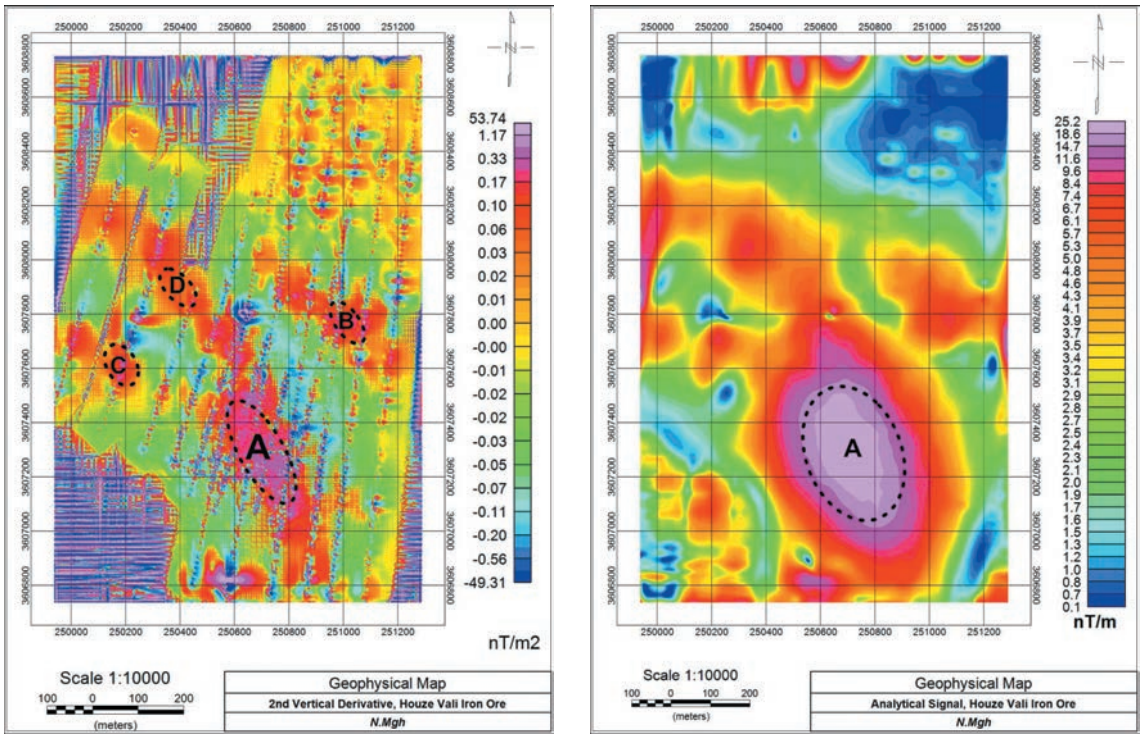

a) b)

Fig. 3 - a) Second vertical derivative map; b) 3D analytic signal of 15 m upward continued TMI data.

Fig. 4a shows the normalized source strength derived from the magnetic gradient tensor (MGT) components, which were calculated from the measured TMI grid, upward continued by 15 m to suppress noise. The NSS map exhibits a prominent high, with peak value of 30 nT/m, over area A. NSS anomalies over the shallow sources have been suppressed by the upward continuation. Fig. 4b shows the gradient tensor element B_{zz} (the vertical gradient of the vertical field component), which generally has the simplest form to interpret. Fig. 4c illustrates the index of dimensionality, i.e., the parameter I of Pedersen and Rasmussen (1990), calculated from the canonical invariants I_1 and I_2, which in turn are calculated directly from the gradient tensor elements. For 2D sources, the parameter I is equal to zero, whereas for a monopole source I = 1 (Pedersen and Rasmussen, 1990). Fig 4c shows that for area A, $0 \leq I \leq 0.6$. This indicates that the source of anomaly A has significant, but limited, strike extent. It is not well represented either by a 2D body or by a point pole source, but has a somewhat intermediate nature.

The strike of elongated sources is indicated by the sub-horizontal eigenvector $\mathbf{v}_3$ that corresponds to the eigenvalue with the smallest absolute value (Beiki and Pedersen, 2010; Beiki, 2013). Fig. 4d shows a rose diagram of estimated strikes within the study area, which indicates fairly consistent strike directions around N60°W.

Euler deconvolution of the TMI data, after upward continuation by 15 m, was implemented using Oasis Montaj software to estimate the depth of the source of anomaly A, assuming a structural index of 0.5, which is reasonable for a thick prismatic body with limited strike extent. Local maxima of the ASA were used to identify a suitable window size for the Euler deconvolution. Fig.

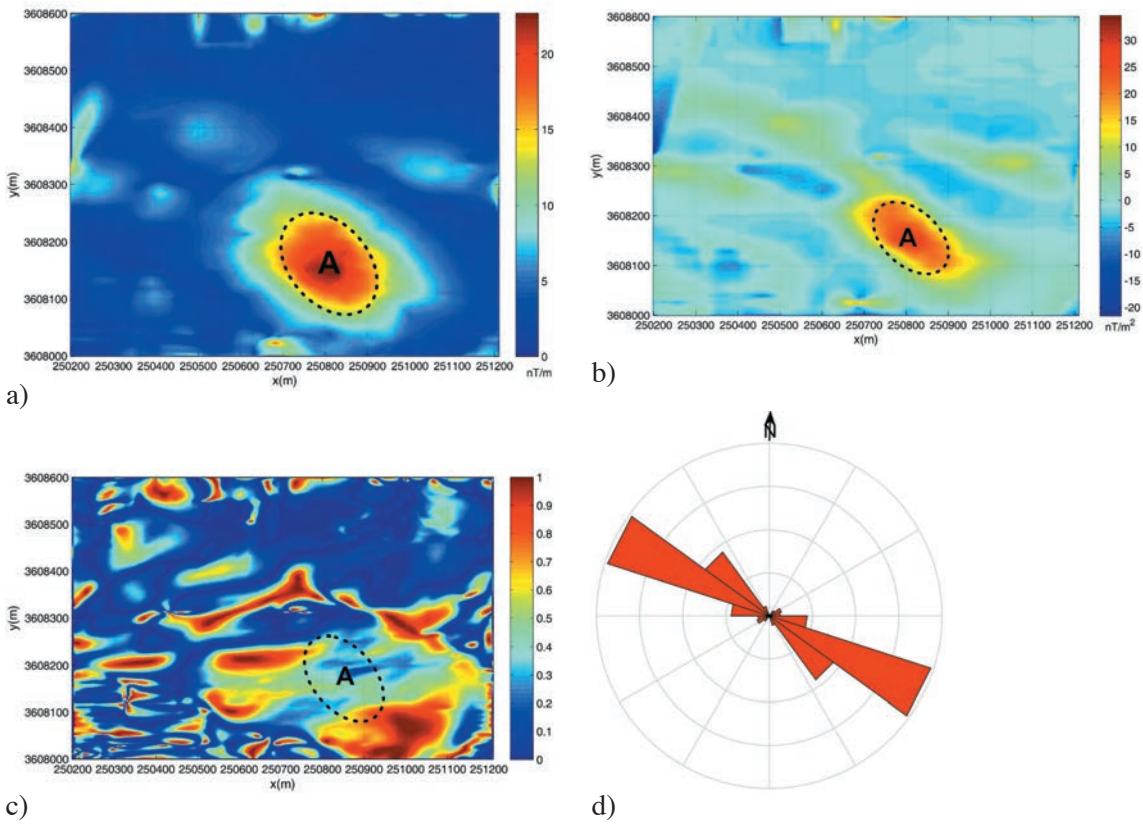

Fig. 4 - a) NSS, nT/m; b) second vertical magnetic components, B_{zz}; c) dimensionality index, I; d) rose diagram of the azimuth of strike.

5a illustrates the depth estimates obtained from Euler deconvolution.

As shown by Fig. 5a, depth estimates for the central portion of anomaly A range from 100 to 150 m, whereas estimated depths for the southern edge of the source are greater than 150 m. Fig. 5a plots the locations of two boreholes that tested the source of anomaly A. Logs of these boreholes (Figs. 5b and 5c) show that magnetite ore was intersected from about 100 m depth and intercalated magnetite ore and monzodiorite intersections continue for tens of metres throughout the rest of the holes.

Structural indices of causative bodies were also estimated from Euler deconvolution of the NSS (Beiki *et al*., 2012). In this method, derivatives of the NSS are calculated on a grid and the inverse problem of the source location is solved in a least-squares sense using data points within a given window. The algorithm of Beiki *et al*. (2012, 2014) was then applied. This algorithm uses the data points within a square window that is centred on a local maximum of the NSS. The depth and the structural index, and their corresponding uncertainties, are estimated from the windowed data (Beiki and Pedersen, 2010). The window size is increased, up to a predefined limit, and parameter estimates corresponding to the window size that minimizes their uncertainties are used in subsequent analysis.

Figs. 6a and 6b show the uncertainties of the estimated depths to source and structural indices of area A, respectively. The rejection criteria, used to discriminate reliable solutions from spurious ones, were as follows:

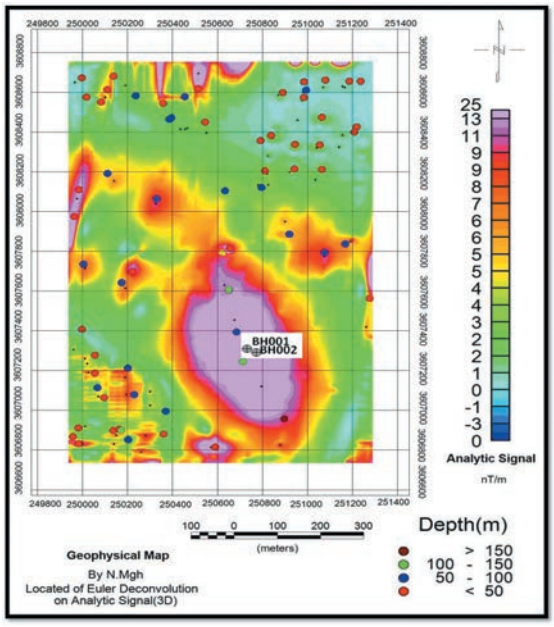

a)

BOREHOLE NUMBER : BH.002		
BOREHOLE COORDINATION :X: 250656, Y :3607496 Z:1116 , INCLINE: 0 ° , AZIMUTH - °		
Depth(m)	Lithology	Distance(m)
0-82.5	Alluvium	82.5
82.5-89	Cream Conglomerate	6.5
89.5-96	MonzoDiorite	6.5
96-98	Mgt-Ore(M)	2
98-104.6	MonzoDiorite	6.6
104.6-121	Mgt-Ore(H)	16.4
121.10_121.50	MonzoDiorite	0.4
121.5_121.9	Mgt-Ore(H)	0.4
121.9_123.5	MonzoDiorite	1.6
123.5_124.20	Mgt-Ore(H)	0.7
124.2_127.3	MonzoDiorite	3.1
127.3_130.8	Mgt-Ore(M)	3.5
130.8_131	Mgt-Ore(H)	0.2
131_138	MonzoDiorite	7
138-143.3	Mgt-Ore(L)	5.3
143.3_147	MonzoDiorite	3.7
147_156.8	Mgt-Ore(L)	9.8
156.8_162	MonzoDiorite	5.2

b)

BOREHOLE NUMBER : BH.001		
BOREHOLE COORDINATION :X: 250681, Y :3607412 Z:1114 , INCLINE: 0 ° , AZIMUTH - °		
Depth(m)	Lithology	Distance(m)
0-86.4	Alluvium	86.4
86.4_89.6	Cream Conglomerate	3.2
89.6-101.5	MonzoDiorite	11.9
101.5-105	Mgt-Ore(M)	3.5
105_107	MonzoDiorite	2
107_109.4	Mgt-Ore(M)	2.4
109.4_111.9	Mgt-Ore(H)	2.5
111.9_119.3	Mgt-Ore(M)	7.4
119.30-128.5	Mgt-Ore(H)	9.2
128.5_129.0	MonzoDiorite	0.5
129-135	Mgt-Ore(M)	6
135-137.1	MonzoDiorite	2.1
137.1_137.30	Mgt-Ore(H)	0.2
137.30_140	Mgt-Ore(L)	2.7

c)

Fig. 5 - a) Located Euler deconvolution of 15 m upward continued TMI data; b) geological description of BH001; c) geological description of BH002.

i. solutions with depth estimates greater than 300 m;
ii. solutions with estimated structural indices smaller than 0.5 and greater than 3;
iii. solutions located outside the corresponding window 330×330 m;
iv. solutions for which errors in the depth estimated from data points within the 20×20 m convolution window exceeded 50%.

Since the rejection criteria are data-dependent, they are based on the available geologic information. The histograms of Figs. 6a and 6b show that the best estimates of the depth and structural index, regarding simultaneous minimization of both uncertainties, are 102 m and 1.41,

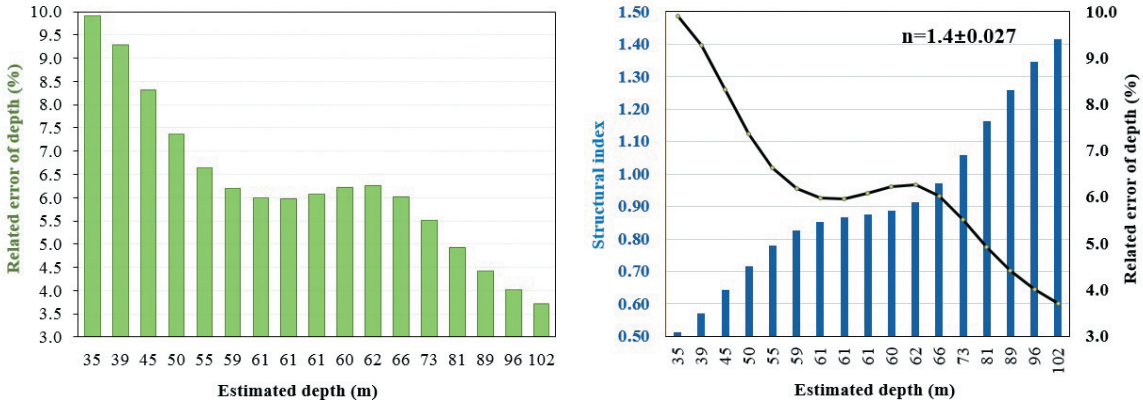

Fig. 6 - Histograms of the uncertainty of the estimated: a) depths; b) structural indices. The solid line shows the uncertainty of the estimated structural indices.

respectively. Note that a structural index of 1.4 for a gradient, such as the NSS, corresponds to a structural index of 0.4 for a field component like the TMI. This depth estimate matches well with the borehole logs and is more accurate that that obtained using the 3D ASA method.

Geological data from drilling and mapping indicate that the iron ore contains minor pyrite, calcite and quartz and is magnetite-rich with variable, but overall very high susceptibility. The country rock in the vicinity of the ore is monzodiorite. At shallow levels, above the base of oxidation, magnetite has been altered to weakly magnetic hematite, limonite and goethite. The source of

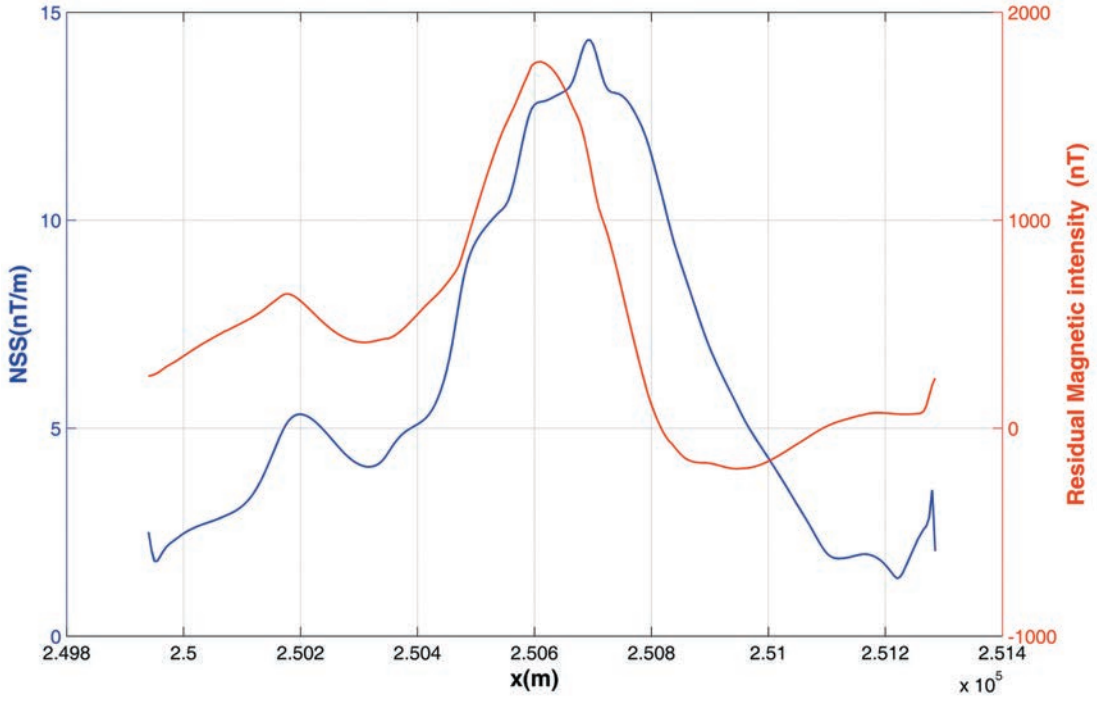

Fig. 7 - A comparison of the maximum of the residual magnetic intensity and the NSS.

anomaly A contains intercalations of magnetite ore and monzodiorite, so it is heterogeneous. The mineralization occurs close to the contact with country rock and appears to result from intense metasomatism that accompanied emplacement of the adjacent igneous intrusion.

Beiki *et al*. (2012) and Clark (2012b) showed that the NSS tends to peak directly above anomaly sources. As can be seen in Fig. 7, the NSS for anomaly A is a symmetric high with a peak that is displaced approximately 100 m from the maximum of the TMI. The residual TMI profile is notably less symmetric. Given the known robustness of the NSS to differences in magnetization direction and to source geometry, locating boreholes on the basis of the NSS is preferable to using TMI maxima. The accuracy of the depth estimate obtained from Euler deconvolution of the NSS confirms that boreholes can be reliably positioned using the NSS.

5. Conclusions

The NSS, calculated from the eigenvalues of the magnetic gradient tensor, usually provides more easily interpretable magnetic source locations in the presence of remnant magnetization. Spatial derivatives of the NSS (calculated from derivatives of the eigenvalues and canonical invariants of the magnetic gradient tensor) can be applied to Euler deconvolution of the NSS, which allows estimating the depth and horizontal location of anomaly sources. Euler deconvolution of the NSS also allows estimating the corresponding structural indices, which constrain the type of source geometry.

For the real data case shown in this paper, ground magnetic TMI data were filtered by upward continuation and by calculation of the second vertical derivative. This was done to identify noise in order to distinguish anomalies due to very shallow sources from anomalies associated with deeper sources. Anomalies B, C and D of Fig. 2 arise from small shallow sources. The major anomaly in this area (A) is associated with magnetite-rich iron ore about 100 m below the surface. According to the dimensionality index and the intermediate eigenvectors of the gradient tensor (associated with the eigenvalue with the smallest absolute value), the strike of the source of anomaly A was N60°W.

Euler deconvolution of TMI data, with an assumed Euler structural index of 0.5 was compared with Euler deconvolution of the NSS, with structural indices estimated using the data. Euler deconvolution of the NSS over anomaly A yielded an estimated structural index of 1.41 for gradients (corresponding to SI = 0.41 for field components) and gave estimated depths around 102 m that were more robust than those obtained from Euler deconvolution of the TMI and were also more consistent with data from two boreholes drilled into the anomaly source.

The drilling data show that the source of anomaly A is a hydrothermal deposit of magnetite-rich iron ore, with minor pyrite, chalcopyrite, azurite and gangue minerals, formed by contact metsomatism within the aureole of an adjacent igneous intrusion. The mineralized zone is heterogeneous, due to intercalated country rocks, but is overall very magnetic. The geometry of the ore body, a tabular body with limited strike extent, is consistent with the inferred Euler structural index.

REFERENCES

Bastani M. and Pedersen L.B.; 2001: *Automatic interpretation of magnetic dike parameters using the analytical signal technique*. Geophys., **66,** 551-561.

Beiki M.; 2010: *Analytic signals of gravity gradient tensor and their application to estimate source location*. Geophys.,**75**, I59-I74.

Beiki M.; 2013: *TSVD analysis of Euler deconvolution to improve estimating magnetic source parameters*: *an example from the Åsele area, Sweden*. J. Appl. Geophys., **90**, 82-91.

Beiki M. and Pedersen L.B.; 2010: *Eigenvector analysis of gravity gradient tensor to locate geologic bodies*. Geophys., **75**, I37-I49.

Beiki M., Clark D.A., Austin J.R. and Foss C.; 2012: *Estimating source location using normalized magnetic source strength calculated for magnetic gradient tensor data*. Geophys., **77**, J23-J37.

Beiki M., Keating P. and Clark D.A.; 2014: *Interpretation of magnetic and gravity gradient tensor data using normalized source strength: a case study from McFaulds Lake, northern Ontario, Canada*. Geophys. Prospect., **62**, 1180-1192.

Blakely R.J.; 1995: *Potential theory in gravity and magnetic application*. Cambridge University Press, Cambridge, UK, 411 pp.

Clark D.A.; 2012a: *New methods for interpretation of magnetic vector and gradient tensor data I: eigenvector analysis and the normalized source strength*. Explor. Geophys., **43**, 267-282.

Clark D.A.; 2012b: *New methods for interpretation of magnetic vector and gradient tensor data II: application to the Mount Leyshon anomaly, Queensland, Australia*. Explor. Geophys., **44**, 114-127.

Clark D.A.; 2014: *Methods for determining remanent and total magnetizations of magnetic sources: a review*. Explor. Geophys., **45**, 271-304.

Dannemiller N. and Li Y.; 2006: *A new method for determination of magnetization direction*. Geophys., **71**, L60-L73.

Gerovska D., Arau'zo-Bravo M.J. and Stavrev P.; 2009: *Estimating the magnetization direction of sources from southeast Bulgaria through correlation between reduced-to-the-pole and total magnitude anomalies*. Geophys. Prospect., **57**, 491-505.

Helbig K.; 1963: *Some integrals of magnetic anomalies and their relation to the parameters of the disturbing body.* Zeit für Geophysik., **29**, 83-96.

Lourenço J.S. and Morrison H.F.; 1973: *Vector magnetic anomalies derived from measurements of a single component of the field*. Geophys., **38**, 359-368.

Nabighian M.N.; 1972: *The analytic signal of two-dimensional magnetic bodies with polygonal cross-section: its properties and use for automated anomaly interpretation*. Geophys., **37**, 507-517.

Nabighian M.N.; 1974: *Additional comments on the analytic signal of two-dimensional magnetic bodies with polygonal cross-section*. Geophys., **39**, 85-92.

Nabighian M.N.; 1984: *Toward a three-dimensional authomatic interpretation of potential field data via generalized Hilbst transforms: Fundamental relations*. Geophys., **49**, 780-786.

Pedersen L.B. and Rasmussen T.M.; 1990: *The gradient tensor of potential field anomalies: some implications on data collection and data processing of maps*. Geophys., **55**, 1558-1566.

Phillips J.D.; 2005: *Can we estimate magnetization directions from aeromagnetic data using Helbig's integrals?* Earth Planets Space, *57*, 681-689.

Pilkington M. and Beiki M.; 2013: *Mitigating remanent magnetization effects in magnetic data using the normalized source strength*. Geophys., **78**, J25-J32, doi:10.1190/GEO2012-0225.1

Roest W.R. and Pilkington M.; 1993: *Identifying remanent magnetization effects in magnetic data*. Geophys., **58**, 653-659.

Roest W.R., Verhoef J. and Pilkington M.; 1992: *Magnetic interpretation using the B-D analytic signal*. Geophys., **57**, 116-125.

Salem A., Ravat D., Ganey T.J. and Ushijima K.; 2002: *Analytic signal approach and its applicability in environmental magnetic investigations*. J. Appl. Geophys., **49**, 231-244.

Schmidt P.W. and Clark D.A.; 1998: *The calculation of magnetic components and moments from TMI: a case study from the Tuckers igneous complex, Queensland*. Explor. Geophys., **29**, 609-614.

Sertcelik I. and Kafadar O.; 2012: *Application of edge detection to potential field data using eigenvalue analysis of structure tensor.* Journal of Applied Geophysics, **84**, 86-94.

Stavrev P. and Gerovska D.; 2000: Magnetic field transforms with low sensitivity to the directin of source magnetization and high centricity. Geophys. Prospect., **48**, 317-340.

Thurston J.B. and Smith R.S.; 1997: *Automatic conversion of magnetic data to depth, dip, and susceptibility contrast using the SPI (TM) method*. Geophys., **62**, 807-813.

Wilson H.S.; 1985: *Analysis of the magnetic gradient tensor: defense research establishment pacific*. Tech. Memorandum, **8**, 5-13.

Appendix - List of symbols.

a-Roman Letter Symbols	
Ax	the analytic signal
B_{zz}	the second vertical of magnetic components
Cm	the magnetic constant
n	the structural index
q	shape factor
r	the location of observation point
r0	the location of source
x, y, z	the Cartesian coordinates
b-Greek Letter Symbols	
λ1, λ2, λ3	the eigenvalues of the gradient tensor
μ	the normalized source strength
Φ, Φ(x,y)	the angle between displacement vectors, the potential field
c-Abbreviations	
ASA	Analytic Signal Amplitude
FFT	Fast Fourier Transform
NSS	Normalized Source Strength
TMI	Total Magnetic Intensity
2D, 3D	Two Dimensional, Three Dimensional

Corresponding author: Banafsheh Habibian Dehkordi
Institute of Geophysics, University of Tehran
North Kargar Street, 14155-6466 Tehran, Iran
Phone: +98 21 88001115; fax: +98 21 88009560; e-mail: bhabibian@ut.ac.ir